
Article:
Pasini, M. orcid.org/0009-0003-6454-0153, Cavazzoni, G. orcid.org/0000-0002-0157-8053, Dall'Ara, E. et al. (4 more authors) (2025) Intervertebral disc degeneration increases surface strain on metastatic vertebrae in compression and flexion but not in torsion. Journal of the Mechanical Behavior of Biomedical Materials, 170. 107109. ISSN: 1751-6161

https://doi.org/10.1016/j.jmbbm.2025.107109

Journal of the Mechanical Behavior of Biomedical Materials 170 (2025) 107109

Contents lists available at ScienceDirect

Journal of the Mechanical Behavior of Biomedical Materials

journal homepage: www.elsevier.com/locate/jmbbm

Intervertebral disc degeneration increases surface strain on metastatic vertebrae in compression and flexion but not in torsion

Margherita Pasini [a], Giulia Cavazzoni [a], Enrico Dall'Ara [b,c], Samuele Luca Gould [a], Christine Le Maitre [b,c], Luca Cristofolini [a], Marco Palanca [a,*]

[a] Department of Industrial Engineering, Alma Mater Studiorum - University of Bologna, Via Umberto Terracini 28, 40131, Bologna, Italy
[b] Division of Clinical Medicine, School of Medicine and Population Health, The University of Sheffield, Barber House, 387 Glossop Road, Sheffield, S10 2HQ, UK
[c] Insigneo Institute, The University of Sheffield, The Pam Liversidge Building, Sheffield, S1 3JD, UK

ARTICLE INFO

Keywords:
Intervertebral disc degeneration
Metastatic vertebrae
Ex vivo biomechanical test
Strain analysis
Digital image correlation (DIC)

ABSTRACT

Despite the fundamental role of intervertebral discs (IVDs) in the biomechanics of the spine, their condition has never been considered among the possible factors affecting the mechanical behaviour of metastatic vertebrae. The structure of the IVDs changes over the course of life, leading to alterations of their biomechanical behaviour. This study aimed to assess if IVD degeneration affects the strains experienced by the adjacent healthy or metastatic vertebrae.

Eight human spine segments consisting of four vertebrae, with a healthy and a metastatic vertebra in the middle and mildly degenerated IVD, were prepared. The segments were biomechanically tested under different loading configurations: axial compression, flexion, and torsion. An enzymatic IVD degeneration was induced by injecting a collagenase solution. The degenerated specimens were tested again, following the same loading protocol. Surface vertebral strains were measured with a 3D-Digital Image Correlation (DIC).

IVD degeneration was found to influence the strain distributions in the adjacent vertebrae. In particular, IVD degeneration resulted in a significant increase of the median compressive strains experienced by the cortical shell of the metastatic vertebrae, in both axial compression (+25.6 %) and flexion (+43.7 %), with larger strains close to the degenerated IVD. Conversely, control vertebral showed less relevant variations between the two conditions. Negligible strain differences were, instead, observed in torsion, for both metastatic and control vertebrae.

This study showed the ability of the healthy vertebrae to withstand loads transmitted in different directions and highlighted the susceptibility of metastatic vertebrae to even minor alterations in boundary conditions.

1. Introduction

The increased life expectancy of oncological patients (Siegel et al., 2020) has highlighted the need for advanced tools to avoid or reduce comorbidities. In the last decade, the morbidity associated with bone metastases has been a critical concern. Up to 70 % of oncological patients with advanced cancers develop bone metastases (Siegel et al., 2012). The spine is the most common anatomical site affected by metastatic bone disease (Coleman, 2001) which negatively affects the microstructure of the vertebrae (Bailey et al., 2020; Burke et al., 2017; Roodman, 2004), impairs the bone homeostasis, and disrupts the bone microstructural optimization by locally increasing (i.e., blastic metastases) or reducing (i.e., lytic metastases) the local bone mineral density (BMD), or by a combination of these two effects (i.e., mixed metastases) (Cavazzoni et al., 2025a; Roodman, 2004). This impaired structure can result in locally degraded mechanical competence (Palanca et al., 2023), reducing the ability of the vertebra to bear loads, and increasing the risk of vertebral fracture (Burke et al., 2017). Understanding how the mechanical behaviour of the vertebra is affected by the metastatic lesions is a critical biomechanical and clinical challenge.

Biomechanical studies have provided insight about the overall mechanical properties of the metastatic vertebrae (Bailey et al., 2020; Palanca et al., 2021, 2023; Costa et al., 2020; Galbusera et al., 2014; Cavazzoni et al., 2025b), showing that the features of the lesion (e.g. metastasis type, size and position) play a fundamental role in defining the mechanical competence of metastatic vertebrae (Bailey et al., 2020; Costa et al., 2020; Palanca et al., 2021).

Very little is known about how the conditions of the intervertebral

* Corresponding author. Department of Industrial Engineering, Alma Mater Studiorum - University of Bologna, Via Umberto Terracini 28, 40131, Bologna, Italy.
E-mail address: marco.palanca@unibo.it (M. Palanca).

https://doi.org/10.1016/j.jmbbm.2025.107109
Received 7 March 2025; Received in revised form 3 June 2025; Accepted 21 June 2025
Available online 21 June 2025

discs (IVDs) affect the mechanical behaviour of the adjacent metastatic vertebrae, although the IVDs are known to provide complementary and synergistic contributions to the complex mechanical behaviour of the spine alongside the vertebrae (Oxland, 2016). In a healthy IVD, a uniform hydrostatic pressure is distributed from the nucleus pulposus (NP) across the underlying vertebrae through the endplates (Keller et al., 1989), while the anulus fibrosus (AF) delivers tensile stress to the vertebral cortical shell (Adams and Roughley, 2006). Over a lifespan, IVDs are exposed to pathological, genetic, traumatic and environmental factors that may trigger degenerative changes (Buckwalter, 1995). IVD degeneration involves structural degradation of the IVDs (Adams and Roughley, 2006; Urban and Roberts, 2003): the overall proteoglycan concentration decreases (Adams and Roughley, 2006; Buckwalter, 1995; Roughley, 2004), causing the dehydration and the depressurization of the NP and altering the collagen chains, leading to a more fibrotic and stiffer NP (Adams and Roughley, 2006; Urban and Roberts, 2003; Roughley, 2004; Adams et al., 1996; Le Maitre et al., 2021). As a consequence, the response of the IVD to mechanical loads (Urban and Roberts, 2003; Adams et al., 1996), and the load transmission across the endplates of the adjacent vertebrae (Pollintine et al., 2004; Raftery et al., 2024) is altered. In particular, the reduction of the hydrostatic pressure in the NP results in a shift of the compressive forces from the inner part of the vertebral endplates towards the AF (Pollintine et al., 2004; Raftery et al., 2024; Adams et al., 2006; Tanaka et al., 2001; Homminga et al., 2012; Neidlinger-Wilke et al., 2014; Techens et al., 2020; Tavana et al., 2021), leading to an increase of the compressive forces transferred to the external cortical shell of the adjacent vertebrae (Raftery et al., 2024).

Recently, the consequences of IVD degeneration in the biomechanical behaviour of human healthy (Raftery et al., 2024) and metastatic spine segments (Cavazzoni et al., 2025b) were explored by means of a combination of microCT and Digital Volume Correlation. IVD degeneration was found to increase the mechanical strains on the trabecular bone of adjacent vertebrae and to be a key factor in determining the failure mode of the adjacent vertebrae, suggesting the importance of considering the level of degeneration in the assessment of the mechanical behaviour of the spine (Cavazzoni et al., 2025b). However, in these studies, i) due to the technological limitations of combining in situ mechanical testing and microCT imaging, the posterior arches were removed from the vertebrae, affecting the load transfer in the spine segments, ii) only a simplified loading configuration (i.e. axial compression in stepwise loading) was investigated excluding the most common failure scenarios, like wedge-fracture.

This evidence highlighted the need to better investigate whether degenerative changes in IVDs influence the mechanical behaviour of the adjacent metastatic vertebrae when loaded with more realistic loading configurations. It has been ascertained that the metastases can weaken the bone (Palanca et al., 2021, 2023) and that IVD degeneration degrades its mechanical competence (Newell et al., 2017). However, the extent of the possible vertebral strain variation due to IVD degeneration during physiological loading is still unknown, whether strains close to failure can be reached by the healthy or metastatic vertebrae, and whether one loading configuration is more demanding than another.

This study aimed to assess the effect of IVD degeneration on the strains experienced by the adjacent healthy and metastatic vertebrae, in different loading configurations, by comparing the strain distribution before and after IVD degeneration.

2. Materials and methods

2.1. Experimental design

Thoraco-lumbar metastatic spine segments with healthy/mild degenerated IVDs were biomechanically tested in the elastic regime, in three different loading configurations. The strains were measured on the external surface of the vertebral bodies and IVDs with Digital Image Correlation (DIC). Enzymatic degeneration of the NP (Cavazzoni et al., 2025b) was induced by injecting a mix of collagenase type II and phosphate buffer solution (PBS) in the central IVD of the spine segments. After degeneration, the specimens were tested again, using the same loading protocol. Effect of the IVD degeneration on the vertebrae was assessed comparing the strains experienced by the vertebrae when loaded by intact IVD (ie. intact condition) and degenerated IVD (ie. degenerated conditions, Fig. 1).

2.2. Donors and specimens' preparation

The study was performed in accordance with the Declaration of Helsinki and approved by the ethical committee of the University of Bologna (Prot. n. 113053, May 10, 2021). Six fresh frozen human spines from donors (Table 1) with a history of spinal metastasis were obtained through an ethically approved donation programme (Anatomic Gifts Registry, Hanover, USA).

The entire spines were imaged with a quantitative Computed Tomography (qCT) (AquilionONE, Canon Medical System Corporation, (Toshiba Medical System Corporation), Otawara, Tochigi, Japan) to assess the metastatic vertebrae. The following scanning protocol optimized for bone was used: voltage 120 kVp, current 200 mA, slice thickness 0.5 mm, in-plane resolution around 0.45 mm (Palanca et al., 2021), with the European Spine Phantom (ESP) for bone density calibration.

The spines were dissected removing fat, muscles and the anterior longitudinal ligaments, without damaging the vertebrae, the posterior facet joints, and the IVDs. Eight segments (Table 1) were harvested from the thoracolumbar spines. Each segment consisted of four vertebrae: a metastatic vertebra and an adjacent control (i.e. without any radiologically relevant sign of metastases) vertebra in the middle, and a cranial and caudal vertebra at the extremities to fix the specimens in the testing machine and apply the loads. Each spine segment was aligned following the protocol used in (Newell et al., 2019; Palanca et al., 2021). The most cranial and caudal vertebrae of the spine segments were partially embedded in Poly-Methyl-Methacrylate (PMMA) (Technovit 4071, Kulzer Technique, Germany). To avoid deterioration of the tissues, the specimens were kept frozen at −28 °C when not in use and subjected to a maximum of three freeze-thaw cycles (Dhillon et al., 2001; Tan and Uppuganti, 2012).

Additionally, to test the repeatability of the mechanical tests, an extra specimen (dummy specimen, not listed in Table 1) with a metastatic (ie. blastic metastases) and a control vertebra was prepared, as reported above, and repeatedly tested only in intact condition.

2.3. Assessment of the metastatic lesion

For each metastatic vertebra, type, size and position of the lesion were determined analysing the qCT images (Table 1) (Palanca et al., 2021).

The type of metastatic lesion (lytic, blastic, or mixed) was determined based on the local BMD variations observed in the qCT images. Lytic lesions were identified as focal regions of decreased BMD compared to the surrounding bone, whereas blastic lesions as regions of increased BMD. Mixed lesions exhibited features of both.

The size of the metastatic lesion was quantified through a manual segmentation, using dedicated image processing software (AMIRA2021, Thermo Fisher Scientific). The procedure is described in (Palanca et al., 2021). Briefly, for each specimen, the volumes of the vertebral body and the metastasis were evaluated manually segmenting the qCT image slice-by-slice. The size of the metastatic lesion was then reported as the percentage of the metastasis volume with respect to the vertebral body volume.

The position of the metastatic lesion was defined with respect to the anatomy of the vertebral body looking at the qCT images.

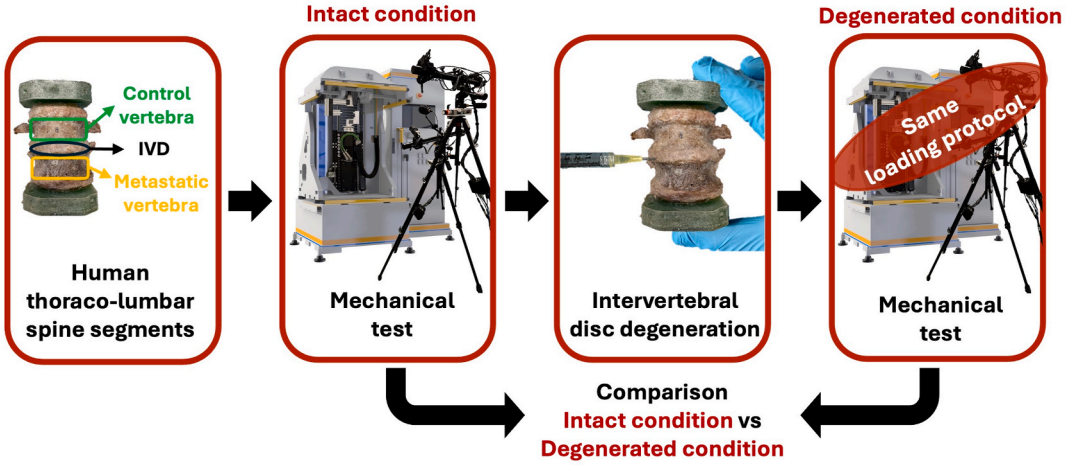

Fig. 1. Study design - human metastatic spine segments with healthy or mildly degenerated IVDs were mechanically tested, in the elastic regime, in three different loading configurations. Controlled enzymatic IVD degeneration was induced in the NP of the central IVD. After IVD degeneration, the specimens were tested again, with the same loading protocol. To quantify the effect of IVD degeneration on vertebrae, the strain distributions were compared between intact and degenerated conditions.

Table 1
Donors' and specimens' details. For each donor, age, sex and primary tumour are reported. For each specimen, the control and metastatic vertebrae are specified. For each metastatic vertebra, the lesion type, size and position are reported.

Donor ID	Age	Sex	Primary tumour	Specimen ID	Segment	Control vertebra	Metastatic vertebra	Lesion type	Lesion size (% of the vertebral body)	Lesion Position
A	79	M	Lung	1	L2-L5	L4	L3	Lytic	2	Top - Posterior Right
B	88	M	Bladder	**2**	T11-L2	T12	L1	Lytic	41	Whole height - Centre/ Posterior
				3	L2-L5	L3	L4	Lytic	30	Whole height - Centre/ Posterior
C	57	F	Breast	**4**	T9-T12	T11	T10	Blastic	100	Whole height - Entire body
D	59	M	Lung	**5**	L3-S1	L4	L5	Blastic	9	Middle/Top - Anterior Right
E	70	F	Breast	**6**	T11-L2	T12	L1	Blastic	7	Bottom/Middle - Anterior Left
F	76	M	Prostate	**7**	T11-L2	T12	L1	Blastic	100	Whole height - Entire body
				8	L2-L5	L3	L4	Blastic	100	Whole height - Entire body

2.4. Assessment of the IVD degeneration

Magnetic Resonance Imaging (MRI) (Ingenia 1.5 T, Philips, The Netherlands) scans were acquired for each specimen to assess the initial degeneration level of the IVDs. To mimic the surrounding soft tissues and increase the signal-to-noise ratio, the specimens were wrapped in a plastic bag filled with physiological solution and imaged using a knee coil. The sagittal T2-weighted Spin-Echo sequence (repetition time (TR) = [3800–4800] ms, echo time (TE) = 100 ms, flip angle = 90°, voxel size (1.8 x 1.5 x 3.5) mm^3) was used. The initial IVD degeneration level was

Table 2
Donors' and specimens IVDs details. For each specimen, the treated IVD, its volume and the injected collagenase solution are specified. The baseline degeneration level is reported for each IVD of each specimen using both the Pfirrmann and the radiographic scores (Liebsch et al., 2022; Pfirrmann et al., 2001; Wilke et al., 2006). All included IVDs exhibited mild degeneration before enzymatic treatment.

Donor ID	Most cranial IVD				Central IVD (i.e. treated IVD)					Most caudal IVD	
	Specimen ID	Segment	Pfirrmann Score[a]	Radiographic Score[b]	Treated IVD	IVD volume (cm^3)	Injected collagenase (cm^3)	Pfirrmann Score[a]	Radiographic Score[b]	Pfirrmann Score[a]	Radiographic Score[b]
A	**1**	L2-L5	1	1	L3L4	22	1.8	1	1	1	1
B	**2**	T11-L2	1	1	T12L1	11	1.6	2	2	2	2
	3	L2-L5	1	1	L3L4	22	3.5	2	2	2	1
C	**4**	T9-T12	2	2	T10T11	8	0.8	2	1	2	1
D	**5**	L3-S1	2	1	L4L5	18	5.0	2	1	1	1
E	**6**	T11-L2	1	1	T12L1	9	0.3	1	2	2	2
F	**7**	T11-L2	2	1	T12L1	13	2.5	1	1	1	2
	8	L2-L5	1	2	L3L4	23	3.3	1	2	2	2

[a] The Pfirrmann score ranges from grade 1 (no degeneration) to grade 5 (severe degeneration).
[b] The radiographic scores range from grade 0 (no degeneration) to grade 3 (severe degeneration).

assessed (Table 2) from MRI images using the Pfirrmann scoring system and its adaptation for lumbar and thoracic IVDs, respectively (Pfirrmann et al., 2001).

In addition, the radiographic scoring systems proposed by Liebsch et al. (2022) for thoracic IVDs and by Wilke et al. (2006) for lumbar IVDs was used. Radiographic images were obtained projecting the 3D qCT images onto the 2D sagittal plane. The three main radiographic signs of IVD degeneration: "Height Loss'', "Osteophyte Formation'' and "Diffuse Sclerosis'' were measured using Horos (Horos Project LGPL 3.0; GNU Lesser General Public License, Version 3), following the procedure reported in (Liebsch et al., 2022; Wilke et al., 2006).

2.5. Artificial IVD degeneration

An enzymatic degeneration to degrade the collagen type I and type II fibres in the NP was induced in the IVD between the control and the metastatic vertebra, following a procedure (Cavazzoni et al., 2025b; Rustenburg et al., 2020; Rivera Tapia et al., 2022) previously validated on human IVDs (Cavazzoni et al., 2025b). A solution of collagenase type II (Gibco™, 125 U/mg) and PBS with a concentration of 2 mg/ml was used since it allowed rapid degeneration of the IVD without damaging the nearby bone tissue (Rustenburg et al., 2020). For the sake of clarity, the nomenclature of the collagenases (i.e. Collagenase type II) does not indicate substrate specificity (Basatvat et al., 2023).

The specimens were preheated at 37 °C for 30 min, wrapped in PBS-soaked gauzes. The collagenase solution was injected within the NP of the IVD, puncturing the AF with a syringe with a 20 G needle until the solution leaked through the injection site. Specimens were double sealed in a plastic bag with PBS-soaked gauzes to keep the IVDs hydrated and placed in a thermostatic bath at 37 °C for 2 h. This incubation time allowed to limit the degeneration to the NP (Cavazzoni et al., 2025b). For each treated IVD, the IVD volume was quantified through manual slice-by-slice segmentation of the MRI images (AMIRA2021, Thermo Fisher Scientific) and the injected collagenase solution recorded (Table 2).

2.6. Biomechanical tests

Before testing, the specimens were thawed in PBS solution overnight at 4 °C and subsequently left at room temperature wrapped in soaked gauze for 1 h to ensure it was fully thawed. A white speckle pattern was prepared on the surfaces of both the vertebral bodies and the IVDs to

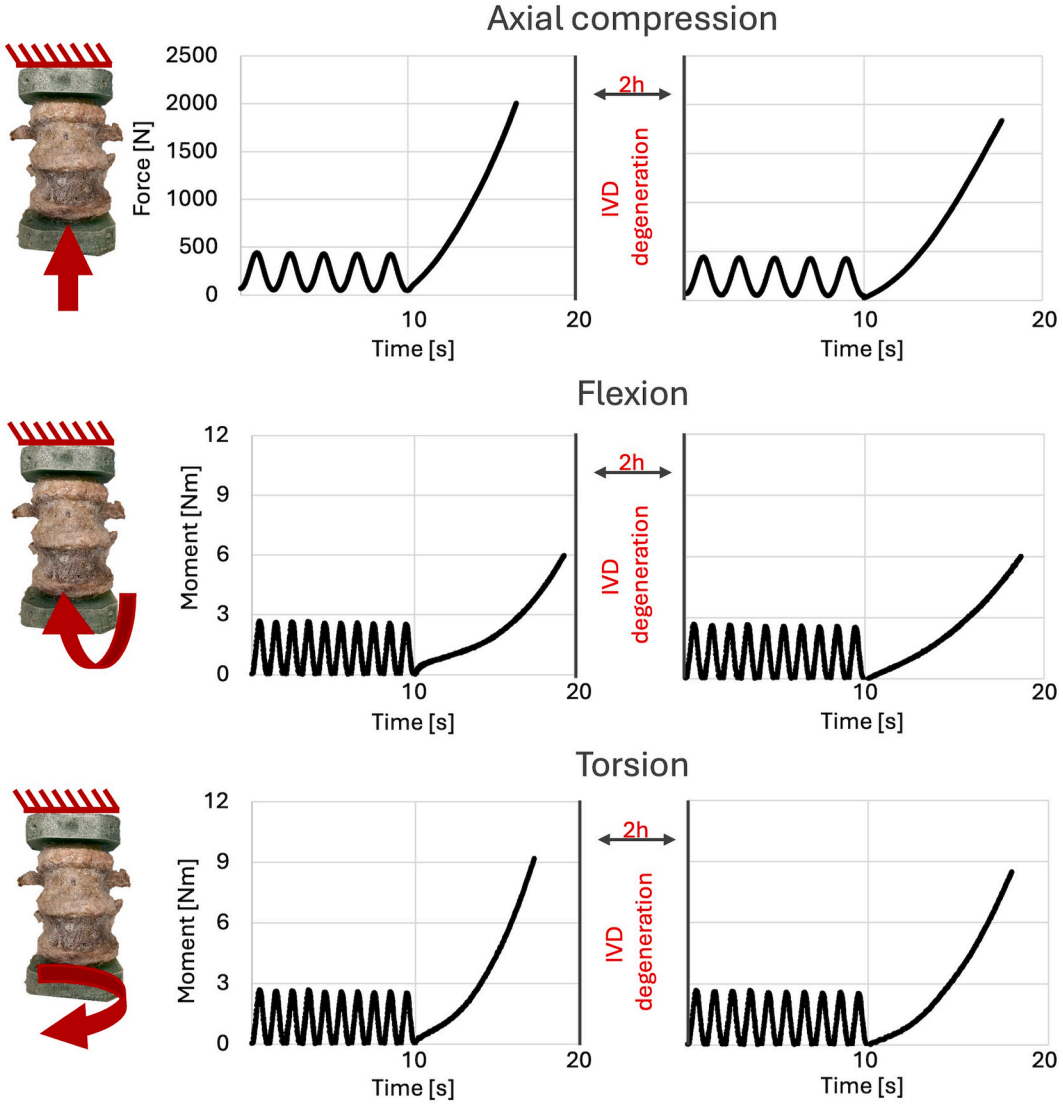

Fig. 2. Example of Load vs Time curves applied to the specimen ID4 (representative specimen) for axial compression (top), flexion (middle) and torsion (bottom), before (left) and after (right) IVD degeneration. Ten preconditioning cycles between 50 N and 300 N in axial compression or between 0.1 Nm and 2.0 Nm for flexion and torsion were applied. Then, a monotonic ramp to the target load was applied in 10 s.

enable the Digital Image Correlation (DIC) measurements over the entire spine segments. A matt white water-based paint (Q250201 Bianco Opaco, Chrèon, Italy) diluted at 40 % with water was sprayed with an airbrush-airgun (AZ3 THE 2, nozzle 1.8 mm, Antes Iwata, Italy). The spraying distance was set to 1m and the pressure to 1 kPa to obtain the desired dot size, and to minimize the scatter of dot dimension (Lionello and Cristofolini, 2014). The median dot size of the obtained speckle pattern was equal to 0.19 mm (3.2 pixels).

The specimens were tested using a state-of-the-art electrodynamic spine simulator (MIB4.0-MAS2-S, MIB, Italy) equipped with a 6-axes load cell (HBM K-MCS10-010-6C, HBK, Germany) (Fig. 2). The specimens were loaded, in the elastic regime, in three loading configurations: axial compression, flexion and torsion. During the mechanical tests, the six components of loads, the displacement along the cranio-caudal direction, and the rotations around the cranio-caudal and medio-lateral axes were acquired at 100 Hz. The full-field strains were measured on the external surface of the vertebral bodies and IVDs using a 3D-DIC system (Aramis Adjustable 12M, Zeiss, Braunschweig, Germany). The DIC system consisted of four cameras (12 MegaPixels 4096 × 3000 pixels, 8 bit) equipped with high-quality 75 mm lenses (f4.5, TitanarB, Schneider-Kreuznach, Germany). The cameras were approximately 1200 mm far from the specimen, with a field of view equal to 260 mm × 190 mm, resulting in a nominal pixel size of 0.063 mm. DIC images were acquired at 25 Hz.

The specimens included in this study exhibited considerable variability in metastatic lesions and bone structure, as well as differences in the spinal levels and donor anthropometry (Table 1, Table 2). To be able to compare results across specimens with different vertebral level and size, the applied load was adapted to induce similar strain values across the sample (Danesi et al., 2016; Palanca et al., 2021). To reach this objective, each specimen was loaded in each configuration until the anterior region of the healthy vertebra reached an average minimum principal strain equal to −2000 με. This value is consistent with the strains typically associated with physiological loads (i.e. range: −1500/-3000 με) (Ehrlich and Lanyon, 2002; Lanyon, 1987), and is approximately 20 % of the failure strain for cortical bone (Bayraktar et al., 2004). For each specimen in each loading configuration, a target load (i.e., force for axial compression and moments for flexion and torsion, Table 3) was identified by increasing the load until the average minimum principal strain measured by the DIC on a 15 × 15 mm^2 surface on the anterior side of the control vertebra reached the target strain level (i.e. −2000 με).

After this tuning, ten preconditioning cycles between 50 N and 300 N for axial compression or between 0.1 Nm and 2.0 Nm for flexion and torsion were applied (Fig. 2). Then, each specimen was preloaded in axial compression at 50N (in all loaded configurations) to grant stability of the specimen inside the testing machine and loaded with a monotonic ramp, at a rate to reach the previously determined target load, in approximately 10 s (Fig. 2).

After artificial IVD degeneration, each specimen was tested again following the same loading protocol, with its target load and rate used before IVD degeneration (Fig. 2), in order to assess the strain variation as a solely consequence of the IVD degeneration. The specimens were tested under the same room temperature and humidity to avoid changes in the mechanical properties of the IVDs.

2.7. Strain measurement uncertainty and repeatability

DIC parameters were set in order to provide the best compromise between measurement spatial resolution and measurement uncertainty (Palanca et al., 2015, 2016, 2018). DIC strain measurement uncertainties were quantified by analysing repeated images acquired in unloaded configuration ("Zero-strain configuration"), as reported in (Palanca et al., 2015). Strains along the axial direction and transverse direction of the spine segments were evaluated on the dummy specimen. Any strain different from zero was accounted as an error. The systematic error was assessed in the axial direction and the transversal direction, separately. They were computed as the average of the strains measured on the measurement points of each spine segment. Similarly, the random error was assessed in the axial and transversal directions, separately, and they were computed as the standard deviation of the strains. Facet size equal to 32 pixels and grid spacing equal to 15 pixels, enabled a measurement spatial resolution equal to approximately 2 mm.

Since the same specimen was tested twice, the intra-specimen repeatability of the testing protocol was assessed on the dummy specimen to account for potential variability arising from specimen handling, rehydration state, and repositioning within the testing machine. The repeatability was quantified by testing the same dummy specimen with the loading protocol described above five times, mounting and dismounting the set up. Prior to each test session, the specimen was rehydrated in PBS at room temperature for an hour and manually repositioned into the testing machine. The maximum and minimum principal strains were computed at the target force. The repeatability of the mechanical test was calculated as the standard deviation of the maximum and minimum principal strains, separately, over the surface of the control vertebra, for all the test repetitions. Repeatability was evaluated on the surface of the control vertebra in order to isolate the measurement from any additional variability.

2.8. Metrics and statistical analysis

For each DIC acquisition, the regions including the anterior surface of the vertebrae and of the IVD were manually selected, making use of the anatomical landmarks, the CT and MRI images.

In this study, vertebrae were grouped into control vertebrae (without any metastatic features visible from the qCT scans) and metastatic vertebrae (accounting for all vertebrae with microstructural alterations due to the metastasis, regardless the type).

The maximum and minimum principal strains were computed on the external surface of the control and of the metastatic vertebral body, for each loading configuration, before (referred to as "intact condition") and after IVD degeneration (referred to as "degenerated condition"). The 3D colour maps of maximum and minimum principal strains on the vertebral surfaces (Supplementary Material 1) and on the intervertebral discs (Supplementary Material 2) were analysed.

Coefficients of variation (CV) of the maximum and minimum principal strains, for each loading configuration, in each condition, were measured for each vertebra to account for the strain heterogeneity.

Table 3
Specimen-specific target loads applied for each loading configuration.

Donor ID	Segment	Control vertebra	Metastatic vertebra	Target force in compression (N)	Target moment in flexion (Nm)	Target moment in torsion (Nm)
A	L2-L5	L4	L3 (lytic)	−850	−4.0	−3.0
B	T11-L2	T12	L1 (lytic)	−1000	−4.4	−9.0
	L2-L5	L3	L4 (lytic)	−1500	−4.0	−4.0
C	T9-T12	T11	T10 (blastic)	−2600	−6.0	−11.0
D	L3-S1	L4	L5 (blastic)	−1070	−5.7	−3.4
E	T11-L2	T12	L1 (blastic)	−1440	−5.0	−6.0
F	T11-L2	T12	L1 (blastic)	−8000	−17.0	−30.0
	L2-L5	L3	L4 (blastic)	−8000	−17.0	−30.0

Moreover, to locally assess the effects of the IVD degeneration, a local analysis was performed on each vertebra. The cortical surface was longitudinally divided into three rectangular regions of interest (ROIs); they were: the "adjacent ROI" which is the region adjacent to the degenerated IVD, the "nonadjacent ROI" which is the farthest region from the degenerated IVD and the "middle ROI" which is the one between the adjacent ROI and nonadjacent ROI. Only adjacent and nonadjacent ROIs were used for the local analysis (Fig. 3) (Palanca et al., 2021).

Differences between the control and metastatic vertebrae in the intact conditions were evaluated for all loading configurations for both the maximum and the minimum principal strains. Strain measurements between intact and degenerated conditions were compared for i) the adjacent control and metastatic vertebrae (pooled data), ii) the control vertebrae, iii) the metastatic vertebrae, iv) the ROIs of control vertebrae adjacent/nonadjacent to the degenerated IVD, v) the ROI of metastatic vertebrae adjacent/nonadjacent to the degenerated IVD.

To assess the normality and homoscedasticity of the data, the Shapiro-Wilk test followed by Levene's test were performed.

Data in the intact condition were compared against the degenerated condition through a non-parametric paired test (Wilcoxon test, for non-normally distributed data) or a parametric paired test (paired *t*-test, for normally distributed data). All statistical analyses were performed in Jamovi (Version 2.3, The Jamovi Project, 2023) , with a significance level set at 0.05. When the alterations were statistically significant, the effects were quantified as percentage variation of strain.

Average maximum and minimum principal strains and strains maps (Supplementary Materials 2) on the intervertebral discs, in the different loading configurations, and different conditions were evaluated.

3. Results

3.1. Repeatability and measurement uncertainties

The strain systematic errors measured on the dummy specimen were 10 με and 37 με in the axial and transversal directions, respectively. The random errors were 148 με and 137 με in the axial and transversal directions, respectively.

The intra-specimen variability in strain measurements was comparable to the estimated strain measurement uncertainties. Specifically, repeatability, quantified as the standard deviation across repeated tests, yielded the following values: under axial compression, the standard deviations for maximum and minimum principal strains were 46 με and 93 με, respectively; during flexion, these values were 68 με and 71 με; and in torsion, they were 171 με and 154 με.

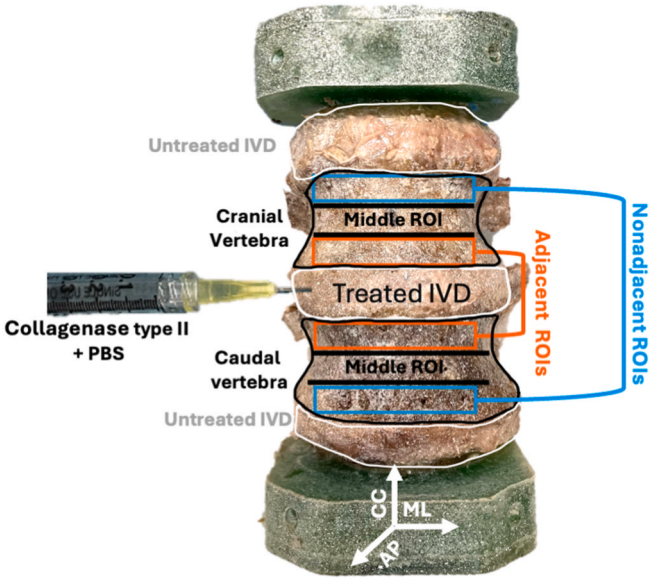

Fig. 3. The ROIs near the degenerated IVD were defined as adjacent ROIs. Similarly, the furthest ROIs were defined as nonadjacent ROIs. The reference system was created using the antero-posterior (AP), medio-lateral (ML) and cranio-caudal (CC) directions.

3.2. Effect of IVD degeneration on adjacent vertebrae

After IVD degeneration, a wider range of the maximum and minimum principal strain magnitude on the surface of the adjacent vertebrae was observed (pooled data for control and metastatic vertebrae), for all the loading configurations (Fig. 4).

Maximum principal strains (pooled data for control and metastatic vertebrae) were larger, after IVD degeneration, in flexion configuration (absolute increase: +29.4 %, $p = 0.05$). Conversely, the maximum principal strains after IVD degeneration were not different in axial compression ($p = 0.10$) and torsion ($p = 0.06$), than in the intact condition (pooled data for metastatic and control vertebrae) (Fig. 4).

Minimum principal strains (pooled data for control and metastatic vertebrae) were significantly larger after IVD degeneration in axial compression (absolute increase: +24.0 %, $p = 0.006$) and flexion (absolute increase: +37.0 %, $p = 0.003$) than in the intact condition, while no difference was found in torsion ($p = 0.21$) (Fig. 4).

The boxes are limited by the first and the third quartile. Mean and median are represented by the cross and the horizontal line, respectively. The whiskers represent the lowest and highest data points in the data set excluding any outliers (dots).

3.3. Effect of IVD degeneration on healthy and metastatic vertebrae

When analysing control and metastatic vertebrae separately, a significant effect of IVD degeneration was only observed in metastatic vertebrae (Fig. 5). The minimum principal strains in the degenerated condition were significantly larger than those in the intact condition: +25.6 % in axial compression ($p = 0.032$) and +43.7 % in flexion ($p = 0.020$), while no statistically significant differences were found in torsion ($p > 0.05$) (Fig. 5). The maximum principal strains were not statistically different in metastatic vertebrae under any of the loading configurations.

By contrast, the control vertebrae did not show any statistically significant difference between the intact and degenerated condition, both for maximum and minimum principal strains, under any of the loading configurations ($p > 0.05$) (Fig. 5).

3.4. Local strain analysis of the vertebrae

The local strain analysis revealed a significant increase, after IVD degeneration, in minimum principal strains under flexion in the ROIs adjacent to the degenerated IVD, for both control and metastatic vertebrae (Fig. 6).

In the control vertebrae, the minimum principal strains in the degenerated condition were significantly larger than those in the intact condition on adjacent ROIs (absolute increase of the magnitude: 36.6 %, $p = 0.023$). Conversely, no differences were found in the nonadjacent ROIs ($p > 0.05$) (Fig. 6). The same effect was observed in the metastatic vertebrae, with an even greater increase on the adjacent ROIs (absolute increase of the magnitude: 67.8 %, $p = 0.040$), while no differences were observed in the nonadjacent ROIs (Fig. 6). No significant effects in minimum principal strains were found for axial compression and torsion loading configuration, in any of the ROIs or vertebral group ($p > 0.05$).

No significant variations were found for the maximum principal strains between intact and degenerated conditions, under any of the loading configurations, for the ROIs adjacent and nonadjacent to the degenerated IVD on both the control and the metastatic vertebrae ($p > 0.05$).

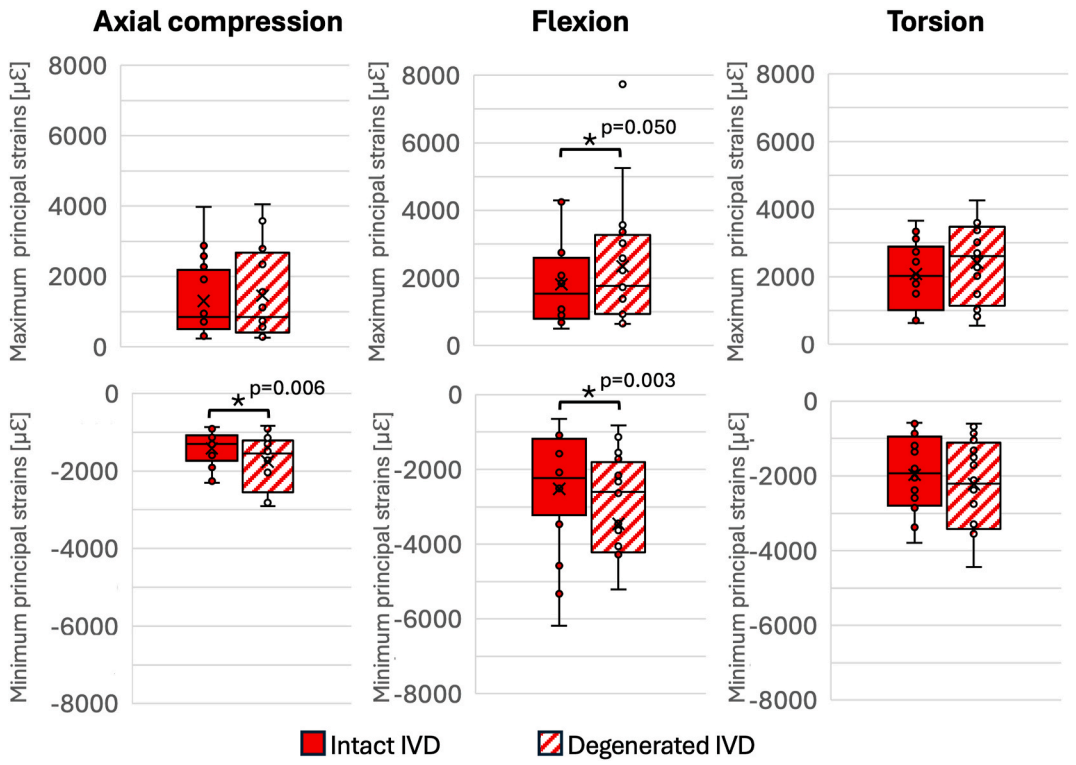

Fig. 4. Maximum and minimum principal strains measured on the entire surface of the adjacent vertebrae (pooled data for control and metastatic vertebrae) to provide an overall comparison of strain magnitude before (intact IVD) and after (degenerated IVD) degeneration of the IVD.

3.5. Strain distribution in the vertebral body

3D strain colour maps were created for each specimen (Supplementary Materials 1 and 2) to qualitatively analyse the spatial distribution of the maximum and minimum principal strains (Fig. 7). A general strain concentration was observed predominantly localized adjacently to the degenerated IVD. This effect was more marked in metastatic vertebrae particularly under axial compression and flexion (Fig. 7 and Supplementary Materials 1), where the strain peaks were observed.

The control vertebrae exhibited negligible differences in the CV of the minimum principal strains between the intact and degenerated conditions, for the different loading configurations ($p = 0.36$ in axial compression, $p = 0.92$ in flexion and $p = 0.93$ in torsion). The metastatic specimens showed negligible differences in the CV for the strain calculated for axial compression ($p = 0.89$) and torsion ($p = 0.11$). Larger differences were found between the CVs calculated for flexion ($p = 0.057$) (Fig. 7 and Supplementary Material 1).

Strain maps of the other specimens are reported in the Supplementary Materials 1 and 2.

4. Discussion

The aim of this study was to evaluate how IVD degeneration affects the strain distributions of the adjacent vertebrae. Eight spine segments including metastatic vertebrae were tested under different loading configurations (i.e. axial compression, flexion and torsion), before and after inducing an artificial IVD degeneration through injection of collagenase type II. DIC was used to measure the strains on the external surface of the IVDs, and of the adjacent control and metastatic vertebral bodies.

The results demonstrated that the IVD degeneration is well tolerated by control (healthy) vertebrae, and it is associated with larger surface strain magnitude on metastatic vertebrae, especially nearby the IVD. In fact, the radiologically healthy vertebrae showed similar strains in the intact and degenerated conditions. A significant increase of the strains was observed, in the degenerated conditions, only on the regions adjacent to the IVD, under flexion, suggesting that IVD degeneration changes the load transfer (i.e. direction and local magnitude) to the healthy vertebrae. Nonetheless, the healthy vertebra can bear it without significant strain alterations. This insight is in line with the observed behaviour of a healthy vertebra loaded in axial compression by a degenerated IVD, where the trabecular bone experienced a different load distribution (Pollintine et al., 2004; Simpson et al., 2001) with consequent increase of the strains in the anterior and peripheral regions (Cavazzoni et al., 2025b; Raftery et al., 2024). Because of this enhanced strain magnitude in the nearby of the endplates, a new trabecular pattern will be designed by the bone remodelling. This could explain why in older spines, reasonably affected by IVD degeneration, the BMD in the trabecular bone adjacent to the endplates is greater than in the central region of the vertebral body (Briggs et al., 2006).

In the metastatic vertebrae, instead, the IVD degeneration further strained the already compromised structure of the vertebra, which experienced strains close to the cortical failure threshold (i.e. -10000 με in axial compression and -7000 με in tension (Bayraktar et al., 2004)). Among the different loading configurations, flexion is the riskiest task for the metastatic vertebra, followed by axial compression (Cavazzoni et al., 2025b). The greatest increase in the minimum principal strains was experienced by the vertebral regions close to the degenerated IVD, whereas the vertebral regions far from the degenerated IVD did not show any relevant variation. These findings can be explained by the altered load distribution within the IVDs after degeneration. In the intact IVDs, the pressurized NP evenly distributes the load to the trabecular bone of the adjacent vertebrae through the entire endplate (Adams et al., 1996; Neidlinger-Wilke et al., 2014; Oxland, 2016; Simpson et al., 2001) and preserves a functional distance between the vertebrae endplates, thus guaranteeing controlled mobility and preserving physiological motion. After IVD degeneration, the path of load transmission is altered: the reduced hydrostatic pressure within the NP causes a shift of the load towards the AF (Adams et al., 2006; Homminga et al., 2012), thus

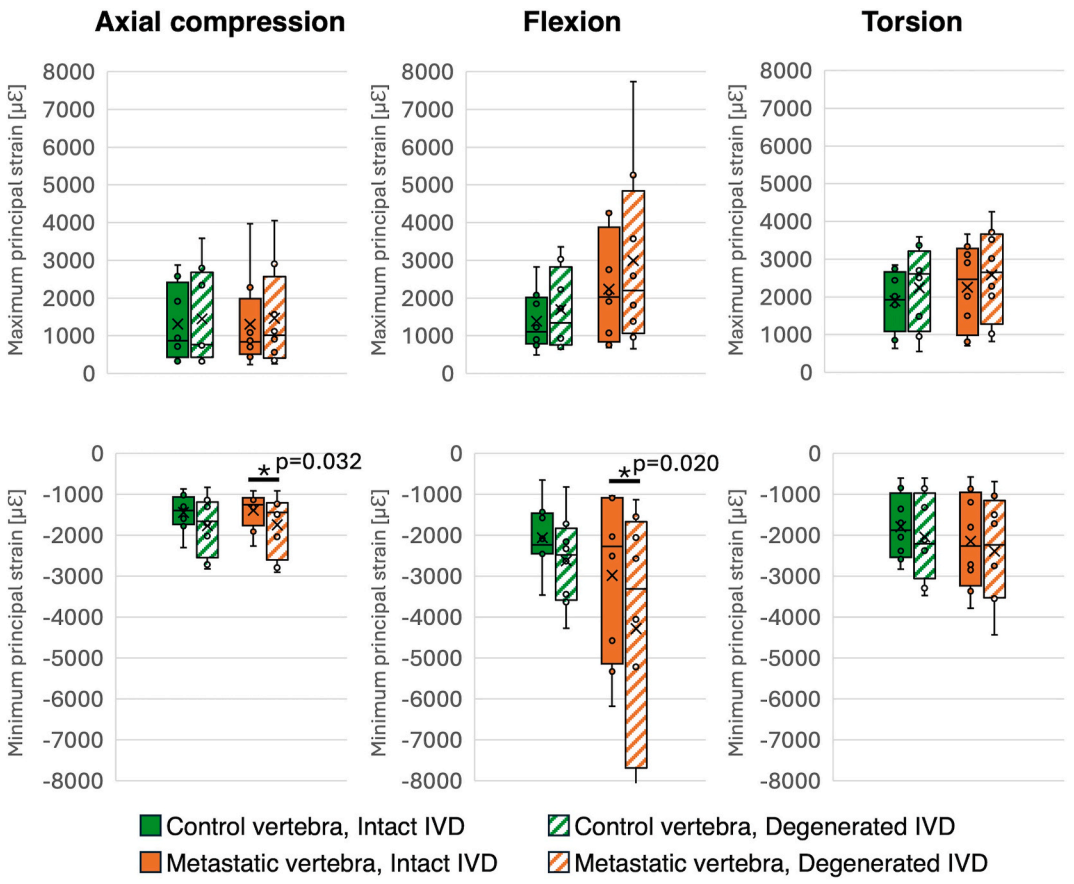

Fig. 5. Maximum and minimum principal strains measured on the entire surface of the vertebral body but differentiates between control and metastatic vertebrae, allowing for an examination of how IVD degeneration affects strain magnitude in each group independently.
The boxes are limited by the first and the third quartile. Mean and median are represented by the cross and the horizontal line, respectively. The whiskers represent the lowest and highest data points in the data set excluding any outliers (dots). Statistically significant differences are highlighted with *.

increasing the load transferred to the external cortical shell of the vertebrae (Kurowski and Kubo, 1986), and reduces the functional distance between the vertebrae endplates, as showed in a previous study performed on similar specimens (Cavazzoni et al., 2025b). This altered load sharing in the vertebrae characterized by a sub-optimal trabecular pattern and reduced competence, like the metastatic ones (Palanca et al., 2023) independently by the metastasis type, can result in failure strains. In both cases of small lesions and large lesions, strain heterogeneity and strain concentrations are expected. Indeed, from a material properties perspective, the higher bone mineral density of the blastic tissue is not always correlated with higher elastic modulus or strength (Stadelmann et al., 2020). From a geometrical point of view, a parallelism could be done considering the vertebroplasty. Several studies (Chevalier et al., 2008; Tan et al., 2020) demonstrated that vertebroplasty is effective only when both endplates are reached by bone cement. Otherwise, the vertebra could result weaker. No differences were observed after IVD degeneration in torsion, both in control and metastatic vertebrae, since torsional loading is primarily governed by the layered collagen structure of the AF (far from the IVD axis), which was not involved in the biochemical degeneration.

This study has some limitations that must be acknowledged. First, although the effectiveness of the enzymatic degeneration used in the present study was validated through visual inspection and histology in a previous study from our group (Cavazzoni et al., 2025b), the degeneration obtained was only partially representative of a real degeneration. Indeed, aside from the localised damage at the needle puncture site, this degeneration model focuses on the NP and does not emulate the structural damage to the outer collagen network of the AF (Cavazzoni et al., 2025b; Rivera Tapia et al., 2022). However, the findings highlighted in this study are still relevant since the degeneration of the NP is the first sign of IVD degeneration (Adams and Roughley, 2006).

Second, the redistribution of the loads between NP and AF occurring *in vivo* as a result of the IVD degeneration triggers a remodelling of the vertebral architecture, with consequently local changes in the bone microstructural properties (Keller et al., 1993). For the healthy vertebrae, this is a major limitation as the actual adaptation cannot be considered in an *in vitro* study, and thus this leads to a bias of the IVD degeneration effects. By contrast, the metastatic vertebrae are characterised by an altered bone homeostasis *per se*, where the systemic disease is the leading cause of the microstructural changes (Bussard et al., 2008).

Third, the sample is characterised by a wide variability (donors' body anthropometry, types of metastases, vertebral level, etc). Despite this, our approach (strain-based condition, and specimen-specific target load) allowed us to reduce the confounding factors, increasing the statistical power. Indeed, each specimen acted as its own control. Data robustness was confirmed by the power analysis. Whereby, based on the physiological strains experienced by the vertebrae and the uncertainty of the experimental pipeline, setting alpha (significance level which is the probability of making a type I error) = 0.05, beta (probability of making a type II error) = 20 %, effect size (minimal differences between degenerated and not degenerated specimens) = 500 με, and standard deviation of the group (the overall uncertainty) = 200 με, the minimum sample size requested for paired analysis was 6 (3 pairs). In this study, 8 specimens were tested twice (degenerated and not degenerated) granting results reliability. Further element of weakness related to our experimental approach is that multiple tests were performed on each specimen. However, the repeatability tests showed that the impact of

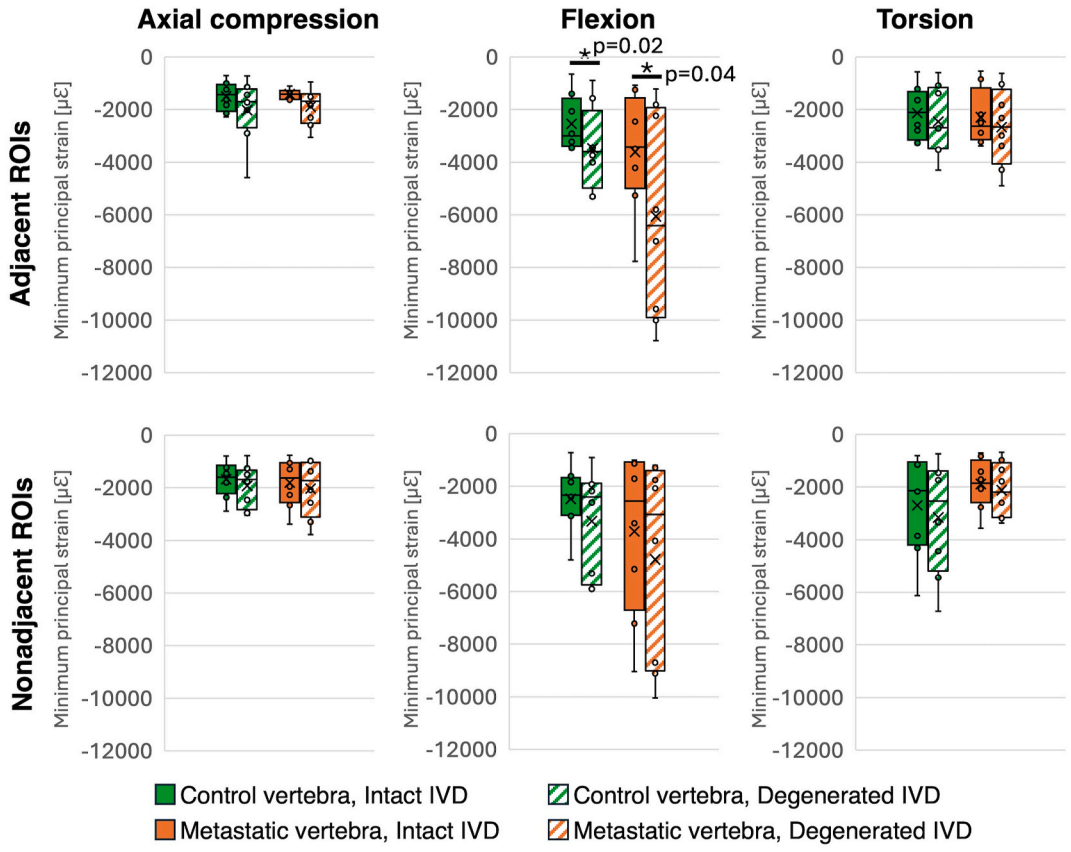

Fig. 6. Minimum principal strains measured on the ROIs adjacent (left) and nonadjacent (right) to the degenerated IVD. This figure also separates healthy and metastatic vertebrae, enabling a detailed assessment of localised strain changes in relation to both IVD degeneration and metastatic involvement.
The boxes are limited by the first and the third quartile. Mean and median are represented by the cross and the horizontal line, respectively. Whiskers represent the lowest and highest data points in the data set excluding any outliers (dots). Statistically significant differences are highlighted with *.

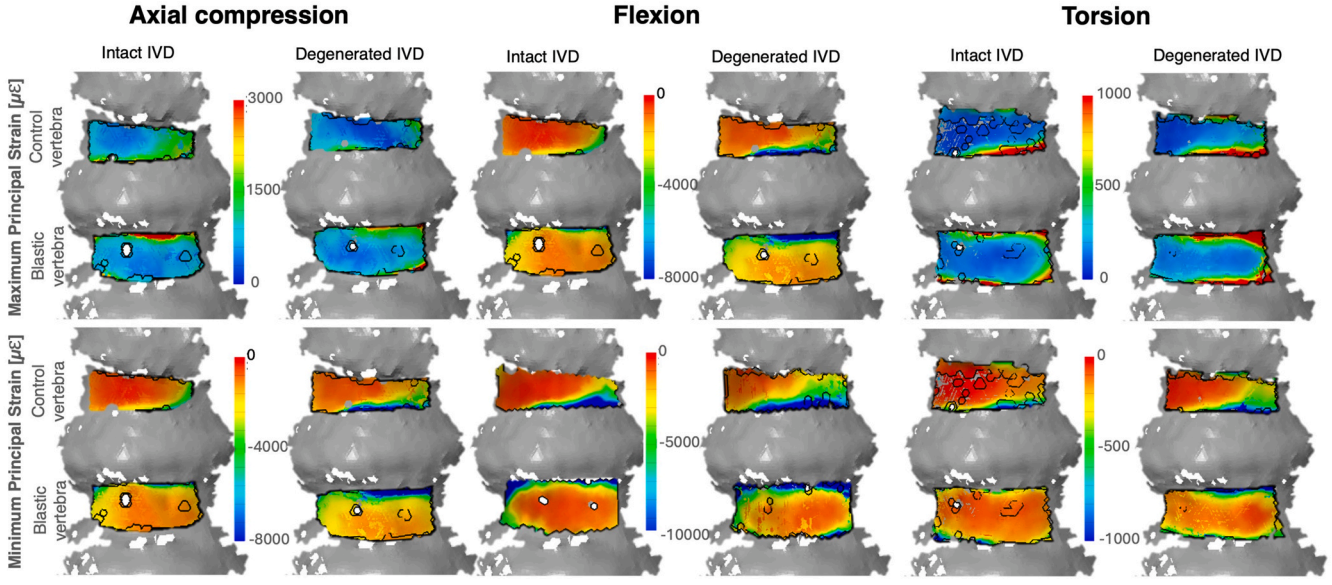

Fig. 7. Maximum and minimum principal strains measured on the external surface of the control and metastatic vertebrae of the specimen ID4 (representative specimen), in axial compression, flexion and torsion configurations. Specific scale bars were adopted for each loading configuration to magnify the effects of the IVD degeneration.

multiple tests on the strain measurements is below the strain measurement uncertainty. Thus, in this study, the observed changes in the mechanical behaviour can be attributed to the effect of the IVD degeneration. More complex loading configurations would have been more representative of daily physiological motor tasks. However, in order to decouple the effects related to the different loading

configurations and reducing the confounding factors, as most of the experimental studies do (Brandolini et al., 2014) and as recommended in the literature (Wilke et al., 1998), we opted for simplified loading configurations (ie. axial compression, flexion and torsion). Another experimental issue could be in the relative position of the metastatic and control vertebrae. In six out of eight cases, the metastatic vertebra is caudal with respect to the control vertebra, and this could bias the results. In fact, the superior endplate is adjacent to the treated IVD, and typically, the superior endplate is thinner than the inferior endplates, showing a high failure likelihood (Zhao et al., 2009). However, as we showed in (Cavazzoni et al., 2025b), failure location in case of degenerated IVD moves from the trabecular bone of the endplate to the cortical shell, reducing the importance of separating the data between the endplates.

The sample was not divided into groups with different types of metastases (i.e. vertebrae with lytic/blastic/mixed metastases). To generalise our findings, the vertebrae were classified as without any visible sign of metastases (i.e. radiographically healthy) and with a compromised trabecular structure (i.e. metastatic). Properly accounting for the combined effect of the different types of metastases and the IVD degeneration would have required a larger sample size. Thus, we refrained from discussing the specific effect of the IVD degeneration on each different metastatic vertebra, and we evaluated if the IVD degeneration level is negligible or not as a potential factor among those for assessing the risk of fracture in metastatic vertebrae. However, this scientific question was partially answered in previous studies (Costa et al., 2020; Galbusera et al., 2018; Palanca et al., 2021), where the effect of the type, size and position of the metastasis on the biomechanics of the vertebra was investigated.

Another limitation is related to the displacement and strain fields measured only on the surface of the specimens. For a more comprehensive and detailed characterization of the effects of IVD degeneration, quantification of the internal strain is necessary. Internal strains can be estimated by using DVC (Cavazzoni et al., 2025b), and findings from the two approaches can be merged. An advantage of DIC over DVC (Cavazzoni et al., 2025b) is that it enables investigation of the strain during tests in a dynamic regime rather than a quasi-static one.

5. Conclusion

This study highlighted the effect of IVD degeneration on the strain experienced by the adjacent healthy and metastatic human vertebrae on the anterior cortical shell. IVD degeneration results in higher strains on the external cortical shell of metastatic vertebrae. In particular, the metastatic vertebrae experience strains close to the failure threshold in regions adjacent to the degenerated IVD, during axial compression and flexion. Therefore, if the metastatic lesion involves the cortical shell near to the IVDs, failure may occur. Conversely, for healthy vertebrae the changes in terms of experienced strains are negligible, in all loading configurations.

CRediT authorship contribution statement

Margherita Pasini: Writing – original draft, Methodology, Investigation, Formal analysis, Data curation, Conceptualization. **Giulia Cavazzoni:** Writing – review & editing, Investigation. **Enrico Dall'Ara:** Writing – review & editing, Supervision, Methodology, Conceptualization. **Samuele Luca Gould:** Writing – review & editing, Methodology. **Christine Le Maitre:** Writing – review & editing, Methodology, Conceptualization. **Luca Cristofolini:** Writing – review & editing, Supervision, Resources, Methodology, Conceptualization. **Marco Palanca:** Writing – review & editing, Supervision, Methodology, Investigation, Funding acquisition, Conceptualization.

Funding sources

The study was partly funded by the AO Spine Knowledge Forum Associate Research Award (AOS-KF-TUM-22-003), by the METASTRA project (EU H2022 grant ID 101080135; UK Horizon Europe Guarantee Extension ID: 10075325) and by the fundamental contribution of Fondazione del Monte of Bologna and Ravenna (MULTIDISC project).

Declaration of competing interest

The authors declare the following financial interests/personal relationships which may be considered as potential competing interests: Marco Palanca reports was provided by AOSpine International. Marco Palanca reports was provided by Horizon Europe. Luca Cristofolini reports was provided by Horizon Europe. Enrico Dall'Ara reports was provided by UK Research and Innovation. Marco Palanca reports was provided by Monte di Bologna and Ravenna Foundation. If there are other authors, they declare that they have no known competing financial interests or personal relationships that could have appeared to influence the work reported in this paper.

Acknowledgement

We sincerely thank Prof. Marco Viceconti for his support and valuable input in this work. Special thanks are also extended to Dr. Giovanni Barbanti-Bròdano and Dr. Paolo Luzi for their help in the classification and selection of specimens.

Appendix A. Supplementary data

Supplementary data to this article can be found online at https://doi.org/10.1016/j.jmbbm.2025.107109.

Data availability

Data will be made available on request.

References

Adams, M.A., Mcnally, D.S., Dolan, P., 1996. "Stress" distributions inside intervertebral discs. The effects of age and degeneration. J. Bone Joint Surg. 78, 8. https://doi.org/10.1302/0301-620x78b6.1287.

Adams, M.A., Pollintine, P., Tobias, J.H., Wakley, G.K., Dolan, P., 2006. Intervertebral disc degeneration can predispose to anterior vertebral fractures in the thoracolumbar spine. J. Bone Miner. Res. 21, 1409–1416. https://doi.org/10.1359/jbmr.060609.

Adams, M.A., Roughley, P.J., 2006. What is intervertebral disc degeneration, and what causes it? Spine 31, 2151–2161. https://doi.org/10.1097/01.brs.0000231761.73859.2c.

Bailey, S., Stadelmann, M.A., Zysset, P.K., Vashishth, D., Alkalay, R.N., 2020. Influence of metastatic bone lesion type and tumor origin on human vertebral bone architecture, matrix quality, and mechanical properties. J. Bone Miner. Res. 37, 896–907. https://doi.org/10.1002/jbmr.4539.

Basatvat, S., Bach, F.C., Barcellona, M.N., Binch, A.L., Buckley, C.T., Bueno, B., Chahine, N.O., Chee, A., Creemers, L.B., Dudli, S., Fearing, B., Ferguson, S.J., Gansau, J., Gantenbein, B., Gawri, R., Glaeser, J.D., Grad, S., Guerrero, J., Haglund, L., Hernandez, P.A., Hoyland, J.A., Huang, C., Iatridis, J.C., Illien-Junger, S., Jing, L., Kraus, P., Laagland, L.T., Lang, G., Leung, V., Li, Z., Lufkin, T., Van Maanen, J.C., McDonnell, E.E., Panebianco, C.J., Presciutti, S.M., Rao, S., Richardson, S.M., Romereim, S., Schmitz, T.C., Schol, J., Setton, L., Sheyn, D., Snuggs, J.W., Sun, Y., Tan, X., Tryfonidou, M.A., Vo, N., Wang, D., Williams, B., Williams, R., Yoon, S.T., Le Maitre, C.L., 2023. Harmonization and standardization of nucleus pulposus cell extraction and culture methods. JOR Spine 6, e1238. https://doi.org/10.1002/jsp2.1238.

Bayraktar, H.H., Morgan, E.F., Niebur, G.L., Morris, G.E., Wong, E.K., Keaveny, T.M., 2004. Comparison of the elastic and yield properties of human femoral trabecular and cortical bone tissue. J. Biomech. 37, 27–35. https://doi.org/10.1016/S0021-9290(03)00257-4.

Brandolini, N., Cristofolini, L., Viceconti, M., 2014. Experimental methods for the biomechanical investigation of the human spine: a review. J. Mech. Med. Biol. 14, 1430002. https://doi.org/10.1142/s0219519414300026.

Briggs, A.M., Wark, J.D., Kantor, S., Fazzalari, N.L., Greig, A.M., Bennell, K.L., 2006. Bone mineral density distribution in thoracic and lumbar vertebrae: an ex vivo study using dual energy X-ray absorptiometry. Bone 38, 286–288. https://doi.org/10.1016/j.bone.2005.07.018.

Buckwalter, J.A., 1995. Aging and degeneration of the human intervertebral disc. Spine 20, 1307–1314. https://doi.org/10.1097/00007632-199506000-00022.
Burke, M., Atkins, A., Kiss, A., Akens, M., Yee, A., Whyne, C., 2017. The impact of metastasis on the mineral phase of vertebral bone tissue. J. Mech. Behav. Biomed. Mater. 69, 75–84. https://doi.org/10.1016/j.jmbbm.2016.12.017.
Bussard, K.M., Gay, C.V., Mastro, A.M., 2008. The bone microenvironment in metastasis; what is special about bone? Cancer Metastasis Rev. 27, 41–55. https://doi.org/10.1007/s10555-007-9109-4.
Cavazzoni, G., Dall'Ara, E., Palanca, M., 2025a. Microstructure of the human metastatic vertebral body. Front. Endocrinol. 15, 1508504. https://doi.org/10.3389/fendo.2024.1508504.
Cavazzoni, G., Pasini, M., Le Maitre, C.L., Dall'Ara, E., Palanca, M., 2025b. Degeneration of the nucleus pulposus affects the internal volumetric strains and failure location of adjacent human metastatic vertebral bodies. Acta Biomaterialia S1742706125000285. https://doi.org/10.1016/j.actbio.2025.01.018.
Chevalier, Y., Pahr, D., Charlebois, M., Heini, P., Schneider, E., Zysset, P., 2008. Cement distribution, volume, and compliance in vertebroplasty: some answers from an anatomy-based nonlinear finite element study. Spine 33, 1722–1730. https://doi.org/10.1097/brs.0b013e31817c750b.
Coleman, R.E., 2001. Metastatic bone disease: clinical features, pathophysiology and treatment strategies. Cancer Treat Rev. 27, 165–176. https://doi.org/10.1053/ctrv.2000.0210.
Costa, M.C., Campello Bresani, L.B., Ryan, M., Rochester, J., Viceconti, M., Dall'Ara, E., 2020. Effect of size and location of simulated lytic lesions on the structural properties of human vertebral bodies, a micro-finite element study. Bone Rep. 12, 100257. https://doi.org/10.1016/j.bonr.2020.100257.
Danesi, V., Erani, P., Brandolini, N., Juszczyk, M.M., Cristofolini, L., 2016. Effect of the in vitro boundary conditions on the surface strain experienced by the vertebral body in the elastic regime. J. Biomech. Eng. 138, 104503. https://doi.org/10.1115/1.4034383.
Dhillon, N., Bass, E.C., Lotz, J.C., 2001. Effect of frozen storage on the creep behavior of human intervertebral discs. Spine 26, 883–888. https://doi.org/10.1097/00007632-200104150-00011.
Ehrlich, P.J., Lanyon, L.E., 2002. Mechanical strain and bone cell function: a review. Osteoporos. Int. 13, 688–700. https://doi.org/10.1007/s001980200095.
Galbusera, F., Qian, Z., Casaroli, G., Bassani, T., Costa, F., Schlager, B., Wilke, H.-J., 2018. The role of the size and location of the tumors and of the vertebral anatomy in determining the structural stability of the metastatically involved spine: a finite element study. Transl. Oncol. 11, 639–646. https://doi.org/10.1016/j.tranon.2018.03.002.
Galbusera, F., Van Rijsbergen, M., Ito, K., Huyghe, J.M., Brayda-Bruno, M., Wilke, H.-J., 2014. Ageing and degenerative changes of the intervertebral disc and their impact on spinal flexibility. Eur. Spine J. https://doi.org/10.1007/s00586-014-3203-4.
Homminga, J., Aquarius, R., Bulsink, V.E., Jansen, C.T.J., Verdonschot, N., 2012. Can vertebral density changes be explained by intervertebral disc degeneration? Med. Eng. Phys. 34, 453–458. https://doi.org/10.1016/j.medengphy.2011.08.003.
Keller, T.S., Hansson, T.H., Abram, A.C., Spengler, D.M., Panjabi, M.M., 1989. Regional variations in the compressive properties of lumbar vertebral trabeculae: effects of disc degeneration. Spine 14, 1012–1019. https://doi.org/10.1097/00007632-198909000-00016.
Keller, T.S., Ziv, I., Moeljanto, E., Spengler, D.M., 1993. Interdependence of lumbar disc and subdiscal bone properties: a report of the normal and degenerated spine. J. Spinal Disord. 6, 106–113. https://doi.org/10.1097/00002517-199304000-00003.
Kurowski, P., Kubo, A., 1986. The relationship of degeneration of the intervertebral disc to mechanical loading conditions on lumbar vertebrae. Spine 11, 726–731. https://doi.org/10.1097/00007632-198609000-00012.
Lanyon, L.E., 1987. Functional strain in bone tissue as an objective, and controlling stimulus for adaptive bone remodelling. J. Biomech. 20, 1083–1093. https://doi.org/10.1016/0021-9290(87)90026-1.
Le Maitre, C.L., Dahia, C.L., Giers, M., Illien-Junger, S., Cicione, C., Samartzis, D., Vadala, G., Fields, A., Lotz, J., 2021. Development of a standardized histopathology scoring system for human intervertebral disc degeneration: an orthopaedic research society spine section initiative. JOR Spine 4, e1167. https://doi.org/10.1002/jsp2.1167.
Liebsch, C., Tao, Y., Kienle, A., Wilke, H.-J., 2022. Validity and interobserver agreement of a new radiographic grading system for intervertebral disc degeneration: part III. Thoracic spine. Eur. Spine J. 31, 726–734. https://doi.org/10.1007/s00586-021-06970-6.
Lionello, G., Cristofolini, L., 2014. A practical approach to optimizing the preparation of speckle patterns for digital-image correlation. Meas. Sci. Technol. 25, 107001. https://doi.org/10.1088/0957-0233/25/10/107001.
Neidlinger-Wilke, C., Galbusera, F., Pratsinis, H., Mavrogonatou, E., Mietsch, A., Kletsas, D., Wilke, H.-J., 2014. Mechanical loading of the intervertebral disc: from the macroscopic to the cellular level. Eur. Spine J. 23, 333–343. https://doi.org/10.1007/s00586-013-2855-9.
Newell, N., Carpanen, D., Grigoriadis, G., Little, J.P., Masouros, S.D., 2019. Material properties of human lumbar intervertebral discs across strain rates. Spine J. 19, 2013–2024. https://doi.org/10.1016/j.spinee.2019.07.012.
Newell, N., Little, J., Christou, A., Adams, M., Adam, C., Masouros, S., 2017. Biomechanics of the human intervertebral disc: a review of testing techniques and results. J. Mech. Behav. Biomed. Mater. 69, 420–434. https://doi.org/10.1016/j.jmbbm.2017.01.037.
Oxland, T.R., 2016. Fundamental biomechanics of the spine—What we have learned in the past 25 years and future directions. J. Biomech. 49, 817–832. https://doi.org/10.1016/j.jbiomech.2015.10.035.
Palanca, M., Barbanti-Bròdano, G., Marras, D., Marciante, M., Serra, M., Gasbarrini, A., Dall'Ara, E., Cristofolini, L., 2021. Type, size, and position of metastatic lesions explain the deformation of the vertebrae under complex loading conditions. Bone 151, 116028. https://doi.org/10.1016/j.bone.2021.116028.
Palanca, M., Brugo, T.M., Cristofolini, L., 2015. Use of digital image correlation to investigate the biomechanics of the vertebra. J. Mech. Med. Biol. 15, 1540004. https://doi.org/10.1142/S0219519415400047.
Palanca, M., Cavazzoni, G., Dall'Ara, E., 2023. The role of bone metastases on the mechanical competence of human vertebrae. Bone 173, 116814. https://doi.org/10.1016/j.bone.2023.116814.
Palanca, M., Marco, M., Ruspi, M.L., Cristofolini, L., 2018. Full-field strain distribution in multi-vertebra spine segments: an in vitro application of digital image correlation. Med. Eng. Phys. 52, 76–83. https://doi.org/10.1016/j.medengphy.2017.11.003.
Palanca, M., Tozzi, G., Cristofolini, L., 2016. The use of digital image correlation in the biomechanical area: a review. Int.Biomech. 3, 1–21. https://doi.org/10.1080/23335432.2015.1117395.
Pfirrmann, C.W.A., Metzdorf, A., Zanetti, M., Hodler, J., Boos, N., 2001. Magnetic resonance classification of lumbar intervertebral disc degeneration. Spine 26, 1873–1878. https://doi.org/10.1097/00007632-200109010-00011.
Pollintine, P., Dolan, P., Tobias, J.H., Adams, M.A., 2004. Intervertebral disc degeneration can lead to "Stress-Shielding" of the anterior vertebral body: a cause of osteoporotic vertebral fracture? Spine 29, 774–782. https://doi.org/10.1097/01.BRS.0000119401.23006.D2.
Raftery, K.A., Kargarzadeh, A., Tavana, S., Newell, N., 2024. Disc degeneration influences the strain magnitude and stress distribution within the adjacent trabecular bone. Front. Bioeng. Biotechnol. 12, 1511685. https://doi.org/10.3389/fbioe.2024.1511685.
Rivera Tapia, E.D., Meakin, J.R., Holsgrove, T.P., 2022. In-vitro models of disc degeneration – a review of methods and clinical relevance. J. Biomech. 142, 111260. https://doi.org/10.1016/j.jbiomech.2022.111260.
Roodman, G.D., 2004. Mechanisms of bone metastasis. N. Engl. J. Med. 350, 1655–1664. https://doi.org/10.1056/NEJMra030831.
Roughley, P.J., 2004. Biology of intervertebral disc aging and degeneration: involvement of the extracellular matrix. Spine 29, 2691–2699. https://doi.org/10.1097/01.brs.0000146101.53784.b1.
Rustenburg, C., Snuggs, J., Emanuel, K., Thorpe, A., Sammon, C., Le Maitre, C., Smit, T., 2020. Modelling the catabolic environment of the moderately degenerated disc with a caprine ex vivo loaded disc culture system. eCM 40, 21–37. https://doi.org/10.22203/eCM.v040a02.
Siegel, R., DeSantis, C., Virgo, K., Stein, K., Mariotto, A., Smith, T., Cooper, D., Gansler, T., Lerro, C., Fedewa, S., Lin, C., Leach, C., Cannady, R.S., Cho, H., Scoppa, S., Hachey, M., Kirch, R., Jemal, A., Ward, E., 2012. Cancer treatment and survivorship statistics, 2012. CA A. Cancer J. Clin. 62, 220–241. https://doi.org/10.3322/caac.21149.
Siegel, R.L., Miller, K.D., Jemal, A., 2020. Cancer statistics, 2020. CA A. Cancer J. Clin. 70, 7–30. https://doi.org/10.3322/caac.21590.
Simpson, E.K., Parkinson, I.H., Manthey, B., Fazzalari, N.L., 2001. Intervertebral disc disorganization is related to trabecular bone architecture in the lumbar spine. J. Bone Miner. Res. 16, 681–687. https://doi.org/10.1359/jbmr.2001.16.4.681.
Stadelmann, M.A., Schenk, D.E., Maquer, G., Lenherr, C., Buck, F.M., Bosshardt, D.D., Hoppe, S., Theumann, N., Alkalay, R.N., Zysset, P.K., 2020. Conventional finite element models estimate the strength of metastatic human vertebrae despite alterations of the bone's tissue and structure. Bone 141, 115598. https://doi.org/10.1016/j.bone.2020.115598.
Tan, J.S., Uppuganti, S., 2012. Cumulative multiple freeze-thaw cycles and testing does not affect subsequent within-day variation in intervertebral flexibility of human cadaveric Lumbosacral spine. Spine 37, E1238–E1242. https://doi.org/10.1097/BRS.0b013e31826111a3.
Tan, L., Wen, B., Guo, Z., Chen, Z., 2020. The effect of bone cement distribution on the outcome of percutaneous vertebroplasty: a case cohort study. BMC Muscoskelet. Disord. 21. https://doi.org/10.1186/s12891-020-03568-9.
Tanaka, N., An, H.S., Lim, T.-H., Fujiwara, A., Jeon, C.-H., Haughton, V.M., 2001. The relationship between disc degeneration and flexibility of the lumbar spine. Spine J. 1, 47–56. https://doi.org/10.1016/S1529-9430(01)00006-7.
Tavana, S., Masouros, S.D., Baxan, N., Freedman, B.A., Hansen, U.N., Newell, N., 2021. The effect of degeneration on internal strains and the mechanism of failure in human intervertebral discs analyzed using digital volume correlation (DVC) and ultra-high field MRI. Front. Bioeng. Biotechnol. 8, 610907. https://doi.org/10.3389/fbioe.2020.610907.
Techens, C., Palanca, M., Éltes, P.E., Lazáry, Á., Cristofolini, L., 2020. Testing the impact of discoplasty on the biomechanics of the intervertebral disc with simulated degeneration: an in vitro study. Med. Eng. Phys. 84, 51–59. https://doi.org/10.1016/j.medengphy.2020.07.024.
The Jamovi project, 2023. Jamovi, Version 2.3.
Urban, J.P., Roberts, S., 2003. Degeneration of the intervertebral disc. Arthritis Res. Ther. 5, 120. https://doi.org/10.1186/ar629.
Wilke, H.J., Rohlmann, F., Neidlinger Wilke, C., Werner, K., Claes, L., Kettler, A., 2006. Validity and interobserver agreement of a new radiographic grading system for intervertebral disc degeneration: part I. Lumbar spine. Eur. Spine J. 15, 720–730. https://doi.org/10.1007/s00586-005-1029-9.
Wilke, H.-J., Wenger, K., Claes, L., 1998. Testing criteria for spinal implants: recommendations for the standardization of in vitro stability testing of spinal implants. Eur. Spine J. 7, 148–154. https://doi.org/10.1007/s005860050045.
Zhao, F.D., Pollintine, P., Hole, B.D., Adams, M.A., Dolan, P., 2009. Vertebral fractures usually affect the cranial endplate because it is thinner and supported by less-dense trabecular bone. Bone 44, 372–379. https://doi.org/10.1016/j.bone.2008.10.048.